Biochimica et Biophysica Acta 1840 (2014) 428–433

Contents lists available at ScienceDirect

Biochimica et Biophysica Acta

journal homepage: www.elsevier.com/locate/bbagen

Synthesizing and staining manganese oxide nanoparticles for cytotoxicity and cellular uptake investigation

Hamed Omid [a,b,*], Mohammad Ali Oghabian [b,c], Reza Ahmadi [a], Narges Shahbazi [d], Hamid Reza Madaah Hosseini [a], Saeed Shanehsazzadeh [c,e], Rashin Namivandi Zangeneh [f]

[a] Department of Materials Science and Engineering, Sharif University of Technology, Azadi Ave., 14588-9694 Tehran, Iran
[b] Research Center for Science & Technology in Medicine, Imam Khomeini Hospital, Tehran, Iran
[c] Department of Medical Physics, Faculty of Medicine, Tehran University of Medical Sciences, Tehran, Iran
[d] Department of Nanobiotechnology, Faculty of Biological Sciences, Tarbiat Modares University, Tehran, Iran
[e] Center for Experimental Radiation Oncology, Cancer Care Center, St George Hospital, Kogarah, NSW, Sydney, Australia
[f] School of Chemistry, University College of Science, University of Tehran, P.O. Box 14155-6455, Tehran, Iran

ARTICLE INFO

Article history:
Received 3 June 2013
Received in revised form 21 August 2013
Accepted 1 October 2013
Available online 7 October 2013

Keywords:
Manganese oxide nanoparticle
Prussian blue staining
MRI contrast agent
Cell uptake
Cytotoxicity

ABSTRACT

Background: For decades, contrast agents have been used to reduce longitudinal (T_1) or transverse (T_2) relaxation times. High toxicity of gadolinium-based contrast agents leads researchers to new T_1 contrast agents. Manganese oxide (MnO) nanoparticle (NP) with the lower peril and good enough signal change ability has been offered as a new possibility for magnetic resonance imaging (MRI).
Methods: The synthesized NPs were investigated for physicochemical and biological properties by X-ray diffraction, Fourier transform infrared spectroscopy, transmission electron microscope, dynamic light scattering (DLS), inductively coupled plasma, enzyme-linked immunosorbent assay, and 3 T magnetic resonance imaging.
Results: Due to physical contact importance of T_1 contrast agents with tissues' protons, extremely thin layer of the surfactant, less than 2 nm, was coated on NPs for aqueous stabilizing. The hydrophilic gentisic acid with low Dalton, around 154, did that role truly. Moreover, decreasing NP size to 5 nm which increases available surface for the proton relaxation is another important parameter to reach an appropriate longitudinal relaxation rate. The NPs didn't reveal any side effects on the cells, and cellular uptake was considerable.
Conclusions: The synthesized NPs represented a promising result in comparison to clinical gadolinium chelates, due to higher r_1 relaxivity and lower toxicity.
General significance: In addition to considerable signal change and cellular uptake, Prussian blue was tried on MnO NPs for the initial time, which can be observed within cells by pale blue color.

1. Introduction

Manganese-enhanced magnetic resonance imaging (MEMRI) has been an interesting subject for researches. Using manganese ion (Mn^{2+}) for the brain T_1 weighted images was common for animal study due to the absorbance ability via voltage-gated Ca^{2+} channels [1], and it is a valuable signal enhancer for the brain cytoarchitecture visualization [2,3]. Some natural products like blueberry and green tea with high concentration of manganese have been previously used as T_1 signal enhancer for gastrointestinal imaging [4].

In the most recent year, MnO NP was studied as a new generation of T_1 contrast agents without nervous and digestive system application limitation. However, there are not various synthesizing methods and biologic perusal about MnO NPs which is the motivation of this work.

The ordinary method for synthesizing MnO NPs is thermal decomposition of manganese acetate in the presence of oleic acid at high temperature [5–9]. In 2010 Baek et al. [10] prepared MnO NPs via hydrothermal process which produces MnO nanocolloid stable in triethylene glycol (TEG) and then makes them water-soluble by use of D-glucuronic acid as surfactant. This nanocolloid was considered as a potential T_1 contrast agent by 7.02 s^{-1} mM^{-1} r_1 relaxivity.

Nowadays by propagating nanotechnology in the biologic field, cellular uptake and cytotoxicity of NPs have become vital parameters which make a vast range of other parameters involved such as size, surfactant, surface charge, and other physicochemical parameters [11]. Two methods for uptake investigation were done in this work. The first plan was staining NPs and employing optical microscope as a qualitative method; and the second one was using inductively coupled plasma to assess concentration of the internalized NPs quantitatively.

Here, we synthesized biocompatible MnO nanocolloid with thin gentisic acid coat by hydrothermal process. It is worthy to mention that gentisic acid as antioxidant excipient is in some pharmaceutical processes. It was consumed, therefore, as a surfactant for improving NP biocompatibility, and making them hydrophilic to be excreted by kidneys [12]. Furthermore, MRI relaxometry demonstrated that the

* Corresponding author. Tel.: +98 9127682780; fax: +98 2634437813.
E-mail address: h_omid@alum.sharif.edu (H. Omid).

0304-4165/$ – see front matter © 2013 Elsevier B.V. All rights reserved.
http://dx.doi.org/10.1016/j.bbagen.2013.10.001

MnO nanocolloid is a potential T_1 contrast agent with a promising future compared with gadolinium chelates.

2. Materials and methods

2.1. Materials

Manganese chloride tetrahydrate ($MnCl_2.4H_2O$), triethylene glycol (TEG) as a solvent, 2,5-dihydroxybenzoic (gentisic) acid as a surfactant, sodium hydroxide (NaOH) as a reducing agent, and potassium hexacyanoferrate ($K_4[Fe(CN)_6].3H_2O$) were all purchased from the Merck. All the chemical reagents were of analytical grade and used as received without further purification. N_2 (99.99%) as flowing gas, and DI water for washing were used.

2.2. Preparation of gentisic acid-coated manganese oxide nanocolloid

The hydrothermal process [10] was employed to synthesize MnO NPs. Initially, 1.98 g of $MnCl_2.4H_2O$ was dissolved in 30 mL solvent. The resultant solution was magnetically stirred at room temperature in a three-necked flask. Separately, 0.8 g NaOH was dissolved in 10 mL solvent, and was added drop-by-drop to the main solution under N_2 gas flow at 200 °C. This condition should be continued for 5 h. Afterward temperature of the solution was lowered to 130 °C and gentisic acid was added. The conclusive solution was stirred overnight. The prepared solution was washed with DI water to remove TEG, unreacted ions and coating ligands. In this step, the green colloid of NPs in TEG turns into a dark brown in water (Fig. 1). The remaining NPs were dispersed in water and fetal bovine serum (FBS) for use in MRI and cell study, respectively. Another part of the synthesizing sample was dried, and the resultant powder was employed for characterizations.

2.3. Characterization

X-ray diffraction technique (XRD, Philips PW 3710, The Netherlands) was performed to recognize NP structure by using Cu K_α radiation ($\lambda = 1.5406$ Å). A transmission electron microscope (TEM, Philips CM100) was employed to determine the average size and morphology of particles. Fourier transform infrared spectroscopy (FTIR, Bruker Vector22, Germany) was carried out to assess surfactant. Hydrodynamic diameter and zeta potential of NPs were determined by a DLS particle size analyzer (Brookhaven *ZetaPlus*, USA). Inductively coupled plasma atomic emission spectroscopy (ICP-AES), and enzyme-linked immunosorbent assay (ELISA reader, Stat Fax-2100 Awareness, Mountain View, CA, USA) were used for the uptake measurement, and the absorbance at 545 nm for the viability test, respectively. The nanocolloid relaxometry was done by a 3 T MRI (MAGNETOM Trio, A Tim System 3T, Siemens, Germany).

2.4. Prussian blue staining

Qualitative evaluation of NPs internalization was done by Prussian blue patch. For staining superparamagnetic iron oxide (SPIO) as a famous NP with lots of applications, the most common material is Prussian blue [13–19]. This staining method makes SPIO NPs blue, and gives suitable contrast in the optical microscopes. Nevertheless, the manganese complex deposition can be monitored by a characteristic light blue color which becomes darker over time. As shown in Fig. 2, at the moment of adding Prussian blue, the color of MnO colloid is negligible than F_3O_4. The MnO colloid's color, however, becomes suitable after 2 h.

$$MnO + 2HCl = Mn^{2+}{}_{aq} + 2Cl^{-}{}_{aq} + H_2O \quad (1)$$

$$2Mn^{2+}{}_{aq} + Fe(CN)_6^{4-}{}_{aq} = Mn_2Fe(CN)_6\downarrow. \quad (2)$$

For this purpose, the washed cells by phosphate buffer saline (PBS) were immersed in a mixture containing an equal volume of 20% aqueous solution of HCl and 10% aqueous solution of potassium ferrocyanide. Kinetics of the above reactions is slow, and takes about 2 h to produce a blue complex.

2.5. Cellular uptake

HeLa cells were obtained from the National Cell Bank of Iran (NCBI), Pasteur Institute, and grown on DMEM F12 medium for 48 h after that, they were exposed to 50 μg/mL MnO NPs for 4 h. Furthermore, protamine sulfate was used as a transfection agent to increase cellular uptake. The used protamine sulfate was prepared as a fresh stock solution of 10 mg/mL in distilled water. Then 20 μg/mL of protamine sulfate was diluted from the stock, and mixed with MnO NPs for 10 min in cell culture medium at room temperature, afterward the solution of NPs and protamine sulfate was added to the existing medium in HeLa cultures.

Quantitative determination of intracellular MnO NP uptake was done by ICP-AES. For this reason, the cells were measured by a hemocytometer, and incubated to 50 μg/mL of the nanocolloid for 4 h. The cells were washed three times thoroughly by PBS solution (pH 7.4) and trypsinized. They were then centrifuged at 1000 *g* for 10 min to form a

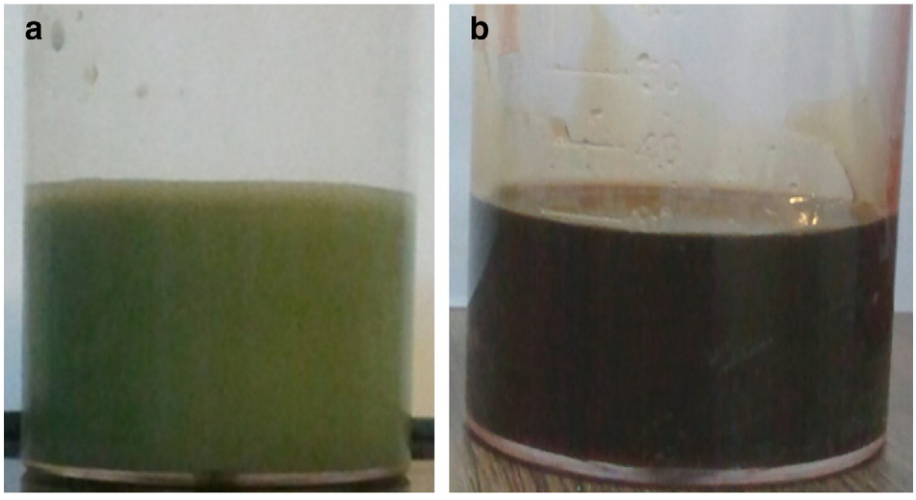

Fig. 1. (a) The synthesized nanocolloid in TEG, and (b) after washing and dispersing in DI water.

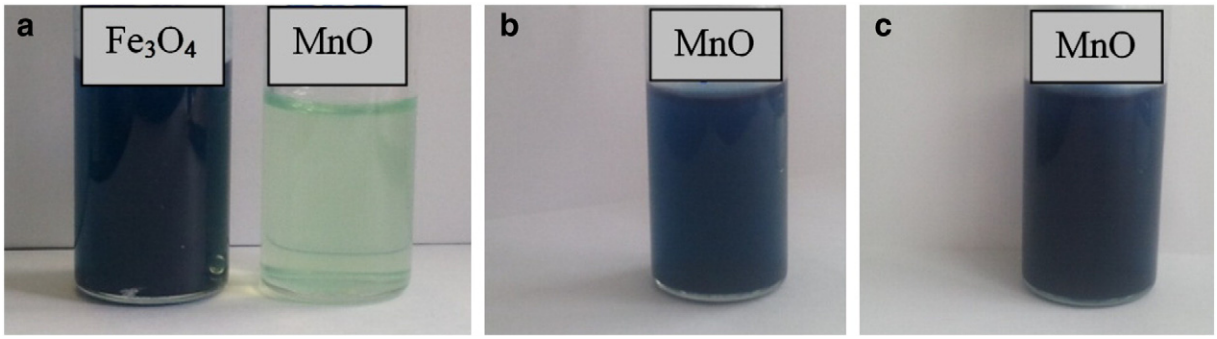

Fig. 2. (a) After adding Prussian blue to Fe_3O_4 and MnO nanocolloids; (b) MnO after 2 h and (c) overnight.

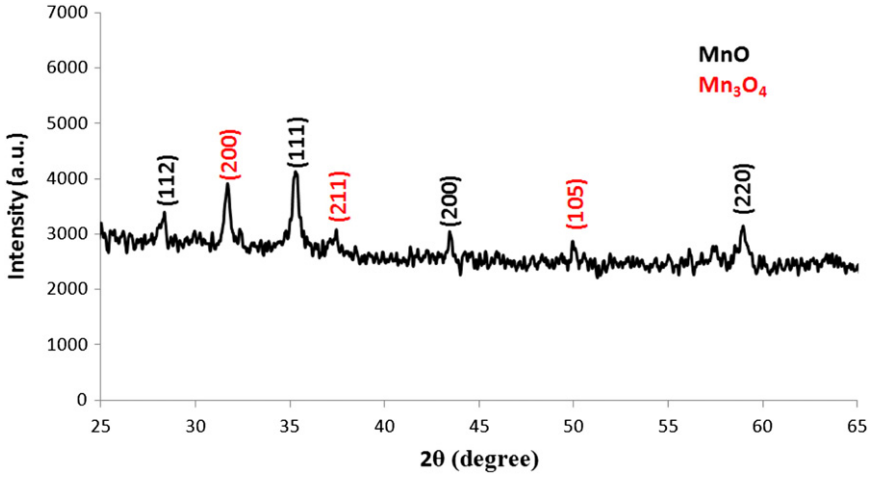

Fig. 3. XRD pattern of the synthesized MnO NPs.

pellet of cells. The cells pellet was dissolved in nitric acid to digest the cells and release Mn^{2+} ions from MnO NPs. Finally, the concentration of Mn^{2+} in the solution was measured by ICP-AES.

2.6. In vitro cytotoxicity

The viability of HeLa cells was estimated using the methylthiazol tetrazolium (MTT) assay [20,21] which measures the ability of metabolically active mitochondria in live cells to reduce a yellow tetrazolium compound to a purple formazan product. The media was removed, and culture media with MTT and PBS were added to each well and cells were incubated for 4 h. Then the media was removed, and the cells were lysed with dimethyl sulfoxide. After dissolving the formazan product, the absorbance at 545 nm was measured using an ELISA reader. Eight replicates were used for three different concentrations. Relative survival was represented as the absorbance of the treated sample per absorbance of the control group.

2.7. MRI and relaxometry

The MRI sample with four different concentrations was prepared in microtubes then all of them were placed in a water container at room temperature (25 °C) to avoid susceptibility artifacts of surrounding air. T_1- and T_2-weighted spin echo (SE) images were attained with variable repetition (TR) and echo (TE) times by a 3-T MR scanner. T_1 maps were attained using six SE images with a fixed TE of 12 ms, and TR values of 5000, 4000, 2000, 1000, 500, and 250 ms. For T_2 maps, five SE images with a fixed TR of 4000 ms, and TE values of 60, 48, 36, 24, and 12 ms were taken. Then both longitudinal (r_1) and transverse (r_2) relaxivities of the contrast agent were calculated according to Eqs (3) and (4):

$$R_1(observed) = R_1(inherent) + r_1 \cdot C \tag{3}$$

$$R_2(observed) = R_2(inherent) + r_2 \cdot C \tag{4}$$

where R_1 and R_2 are reciprocal of T_1 and T_2 relaxation time, respectively. *Inherent* and *observed* denote tissue relaxation without and with contrast agent, respectively. *C* is contrast agent concentration.

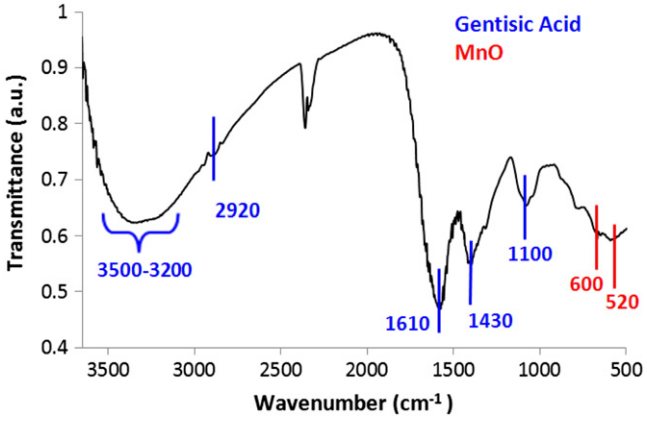

Fig. 4. FTIR spectrum of gentisic acid coated manganese oxide nanoparticles.

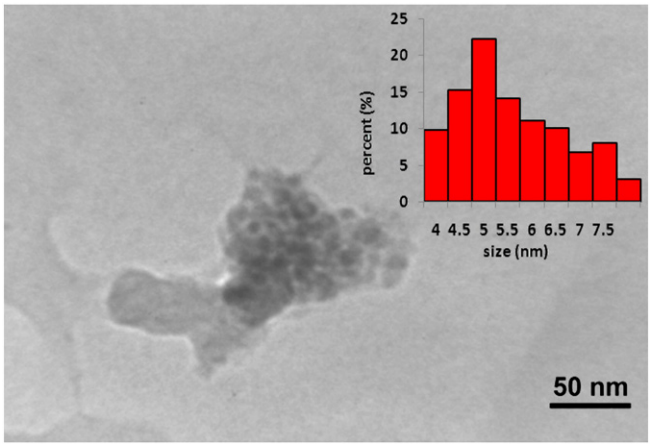

Fig. 5. TEM micrograph and size dispersity of the nanoparticles.

3. Results and discussion

Fig. 3 illustrates the XRD plot of the synthesized NPs. Characteristic peaks are matched with standard face-centered cubic MnO (JCPDS 78-0424) and tetragonal phase of γ-Mn_3O_4 (JCPDS Card, No. 80-0382). For reducing γ-Mn_3O_4 phase, protection should be done to prevent excess oxidation, but drying the sample to produce powder for XRD causes unwanted oxidation. Accordingly, the synthesized nanocolloid, before drying, has a negligible γ-Mn_3O_4.

In Fig. 4, the surface coating was assessed by FTIR spectrum of the sample. The C–O, C═C, C═O, and C–H stretch at 1100, 1430, 1610, and 2920 cm^{-1}, respectively. The O–H characteristic absorptions are between 3200 and 3500 cm^{-1}. The mentioned bonds verify gentisic acid coating. The two peaks of 520 and 600 cm^{-1} with the low intensity representing the Mn–O bond [22]. To the best of our knowledge, mineral structures like MnO have stronger bonds, and weaker vibrations that decrease peak intensity in FTIR spectra. Moreover, conjugation of the surfactant to a mineral particle shifts the surfactant peaks to the lower wavenumbers.

TEM micrograph and NP size dispersity are shown in Fig. 5. According to TEM results, NP core size was measured and percentage of NPs in each size period was plotted which shows 5 nm as the mode size. NP size and hydrodynamic radius has an essential role in cellular uptake and biodistribution [11]. Cellular uptake usually increases with decreasing NP size. However, Jiang et al. [23] showed that a very small NP may not be able to trigger the endocytosis process due to the lack of interaction with adequate receptors. Hence, several NPs should be accumulated on the cell membrane to start pit formation.

Fig. 6 illustrates the hydrodynamic diameter and zeta potential of NPs. The average hydrodynamic diameter of NPs as shown is 7.7 nm. In accord with the 5 nm core size, the thickness of the coating is less than 1.5 nm which is so thin and appropriate for T_1 contrast agents. As we know T_1 contrast agents have spin–lattice relaxation procedure, and need physical contact with environmental protons. Moreover, electrophoretic mobility and zeta potential were analyzed in three runs by a DLS device, and the mean zeta potential −15.91 mV was reported. Some NPs with positive surface charge are identified by reticuloendothelial system (RES) and mononuclear phagocytic system as opsonins which lead these NPs to the liver and spleen [11,24]. Many NPs with negatively charged groups and zeta potential around −30 to −50 mV are stable in physiological systems. They are however covered instantaneously by biological fluid proteins which considerably increases hydrodynamic diameter, and ruins the targeting capabilities of surface functions [11,25,26]. Thus NPs with small negative zeta potential (−10 to −20 mV) should have better performance in physiological conditions by adsorbing the slight protein corona shell and negligible size tolerance. Furthermore, the negative zeta potential should attract more protons for adsorbing on the unpaired S-state of manganese ions. Mn ions which exist in NP surface are operative of proton relaxation, and small size of NPs increases their surface.

Fig. 7 shows that more than 80% of the HeLa cells turned positive upon Prussian blue staining after 4 h of incubation with MnO NPs. Prussian blue staining demonstrated manganese-containing sites as light

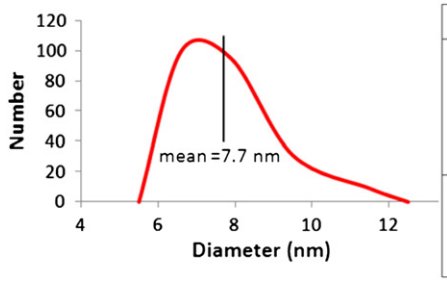

Run	Mobility ($10^{-4}cm^2/s.V$)	Zeta Potential (mV)	Rel. Residual
1	−1.10	−15.47	0.0155
2	−1.12	−15.74	0.0212
3	−1.17	−16.52	0.0122
Mean	−1.13	−15.91	0.0163
Std. Error	0.02	0.32	0.0026
Combined	−1.12	−15.71	0.0096

Fig. 6. Hydrodynamic size, and zeta potential of the synthesized sample.

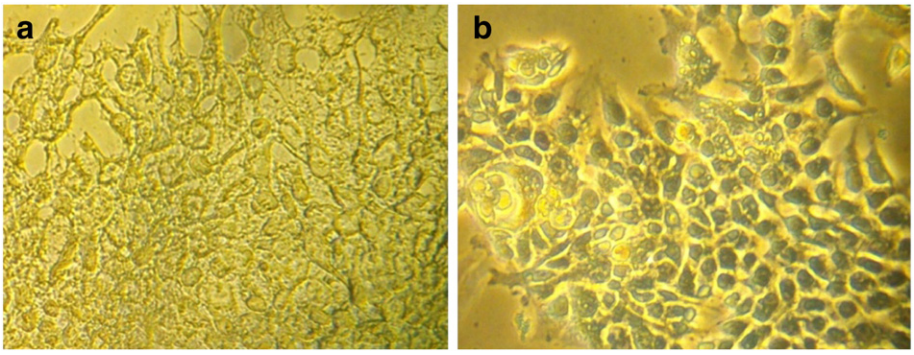

Fig. 7. HeLa cells (a) before and (b) after Prussian blue staining at the same magnification.

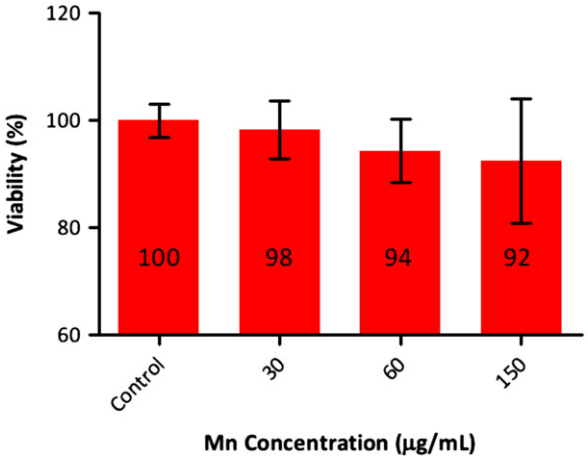

Fig. 8. MTT assay of the MnO NPs on HeLa cell line.

blue spots in the cytoplasm. In addition, manganese concentration for around 500,000 cells which was measured by ICP-AES was 0.47 ppm (0.94 pg/cell), and when protamine sulfate was used this result turns into 1.46 ppm (2.92 pg/cell). It demonstrates that the transfection agent increases cellular uptake up to three times. Kim et al. [27] had labeled adipose-derived mesenchymal stem cells by mesoporous silica-coated hollow manganese oxide NPs, and reached to 0.35 and 0.09 pg/cell uptake with electroporation and incubation, respectively. Accordingly, our uptake without electroporation and its side effects was worthy. The small hydrodynamic size of the MnO NPs is the most important key for uptake enhancing.

MTT assay was done for three different concentrations of manganese. The same cells without MnO nanocolloid treatment were used as a control, and each experiment was repeated for eight times to enhance accuracy of data. As shown in Fig. 8 up to 150 μg/mL of manganese, no side effect was observed in HeLa cells. The most important point is that manganese ions are toxic. Hence, the synthesized nanocolloid should be washed by DI water thoroughly. Moreover, gentisic acid as an existing phenolic acid in wine was employed for improving particles' biocompatibility.

Fig. 9 depicts T_1 and T_2 weighted images of the synthesized nanocolloid that reveals dose-dependent contrast. It is obvious that MnO NPs are able to change both r_1 and r_2 relaxivities. Five unpaired electrons in the d-orbital and high electron spin relaxation time make MnO suitable as a T_1 contrast agent. Additionally, being antiferromagnetic instead of paramagnetic, the common form of positive contrast agents, gives a small amount of magnetic dipole which increases r_2.

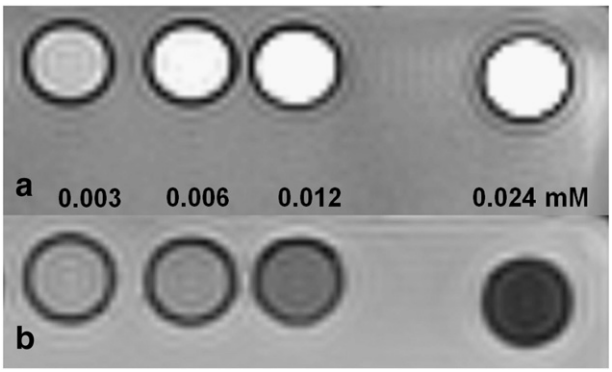

Fig. 9. (a) T_1-weighted (T_R/T_E:1000/12) and (b) T_2-weighted (T_R/T_E:4000/60) images for the prepared contrast agent as a function of Mn concentration.

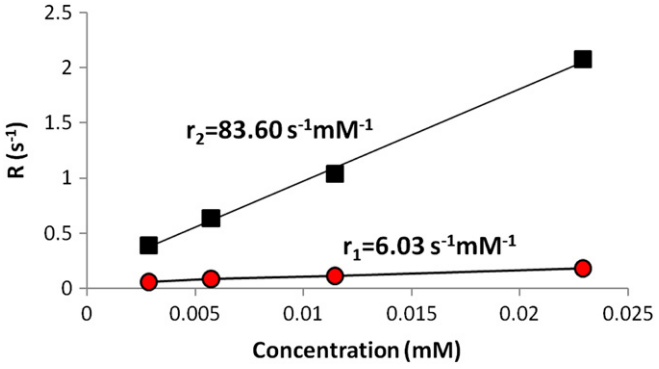

Fig. 10. R_1 and R_2 relaxations of the prepared contrast agent as a function of Mn concentration.

The plots of R_1 and R_2 relaxations versus Mn concentration were drawn in Fig. 10, and from their slope the nanocolloid r_1 and r_2 relaxivities were acquired at 6.03 and 83.6 $s^{-1}\,mM^{-1}$, respectively.

4. Conclusion

In this paper we have used various characterization techniques to deduce the physical and biological properties of the synthesized MnO NPs. The NPs' r_1 relaxivity is 6.03 $s^{-1}\,mM^{-1}$ which is more promising than the Gd-DOTA, a clinically usable T_1 contrast agent, with 3.5 $s^{-1}\,mM^{-1}$ r_1 relaxivity in 3T. The small size of NPs (5 nm) and thin layer of hydrophilic surfactant (less than 1.5 nm) are two key parameters to reach satisfying relaxivity. MTT assay reveals that NPs have good biocompatibility, and can be used without serious side effects. In addition to low cytotoxicity, uptake of 2.92 pg/cell with protamine sulfate transfection was obtained which is a considerable result based on the available literature.

References

[1] S.J. Jackson, R. Hussey, M.A. Jansen, G.D. Merrifield, I. Marshall, A. MacLullich, J.L.W. Yau, T. Bast, Manganese-enhanced magnetic resonance imaging (MEMRI) of rat brain after systemic administration of MnCl2: hippocampal signal enhancement without disruption of hippocampus-dependent behavior, Behav. Brain Res. 216 (2011) 293–300.
[2] A.P. Koretsky, A.C. Silva, Manganese-enhanced magnetic resonance imaging (MEMRI), NMR Biomed. 17 (2004) 527–531.
[3] A.C. Silva, J.H. Lee, I. Aoki, A.P. Koretsky, Manganese-enhanced magnetic resonance imaging (MEMRI): methodological and practical considerations, NMR Biomed. 17 (2004) 532–543.
[4] Y. Mino, K. Yamada, T. Takeda, O. Nagasawa, Metal-containing components in medicinal plants. III. Manganese-containing components in *Theae folium* as oral magnetic resonance imaging contrast materials, Chem. Pharm. Bull. (Tokyo) 44 (1996) 2305–2308.
[5] M. Yin, S. O'Brien, Synthesis of monodisperse nanocrystals of manganese oxides, J. Am. Chem. Soc. 125 (2003) 10180–10181.
[6] Y.C. Lee, D.Y. Chen, S.J. Dodd, N. Bouraoud, A.P. Koretsky, K.M. Krishnan, The use of silica coated MnO nanoparticles to control MRI relaxivity in response to specific physiological changes, Biomaterials 33 (2012) 3560–3567.
[7] M.A. Morales, R. Skomski, S. Fritz, G. Shelburne, J.E. Shield, M. Yin, S. O'Brien, D.L. Leslie-Pelecky, Surface anisotropy and magnetic freezing of MnO nanoparticles, Phys. Rev. B 75 (2007) 134423.
[8] H.B. Na, J.H. Lee, K. An, Y.I. Park, M. Park, I.S. Lee, D.H. Nam, S.T. Kim, S.H. Kim, S.W. Kim, K.H. Lim, K.S. Kim, S.O. Kim, T. Hyeon, Development of a T1 contrast agent for magnetic resonance imaging using MnO nanoparticles, Angew. Chem. Int. Ed. 46 (2007) 5397–5401.
[9] M.F. Bennewitz, T.L. Lobo, M.K. Nkansah, G. Ulas, G.W. Brudvig, E.M. Shapiro, Biocompatible and pH sensitive PLGA encapsulated MnO nanocrystals for molecular and cellular MRI, ACS Nano 5 (2011) 3438–3446.
[10] M.J. Baek, J.Y. Park, W. Xu, K. Kattel, H.G. Kim, E.J. Lee, A.K. Patel, J.J. Lee, Y. Chang, T.J. Kim, J.E. Bae, K.S. Chae, G.H. Lee, Water-soluble MnO nanocolloid for a molecular T 1 MR imaging: a facile one-pot synthesis, in vivo T 1 MR images, and account for relaxivities, ACS Appl. Mater. Interfaces 2 (2010) 2949–2955.
[11] M. Mahmoudi, I. Lynch, M.R. Ejtehadi, M.P. Monopoli, F.B. Bombelli, S. Laurent, Protein-nanoparticle interactions: opportunities and challenges, Chem. Rev. 111 (2011) 5610–5637.
[12] G. Levy, T. Tsuchiya, Salicylate accumulation kinetics in man, N. Engl. J. Med. 287 (1972) 430–432.
[13] X.-Q. Zhang, S.-W. Gong, Y. Zhang, T. Yang, C.-Y. Wang, N. Gu, Prussian blue modified iron oxide magnetic nanoparticles and their high peroxidase-like activity, J. Mater. Chem. 20 (2010) 5110–5116.

[14] S. Shanehsazzadeh, M. Oghabian, B. Allen, M. Amanlou, A. Masoudi, F. Daha, Evaluating the effect of ultrasmall superparamagnetic iron oxide nanoparticles for a long-term magnetic cell labeling, J. Med. Phys. 38 (2013) 34–40.
[15] Y. Hou, Y. Liu, Z. Chen, N. Gu, J. Wang, Manufacture of IRDye800CW-coupled Fe3O4 nanoparticles and their applications in cell labeling and in vivo imaging, J. Nanobiotechnol. 8 (2010) 25.
[16] A. Masoudi, H.R. Madaah Hosseini, M.A. Shokrgozar, R. Ahmadi, M.A. Oghabian, The effect of poly(ethylene glycol) coating on colloidal stability of superparamagnetic iron oxide nanoparticles as potential MRI contrast agent, Int. J. Pharm. 433 (2012) 129–141.
[17] S. Ju, G. Teng, Y. Zhang, M. Ma, F. Chen, Y. Ni, In vitro labeling and MRI of mesenchymal stem cells from human umbilical cord blood, Magn. Reson. Imaging 24 (2006) 611–617.
[18] L. Liu, T.K. Hitchens, Q. Ye, Y. Wu, B. Barbe, D.E. Prior, W.F. Li, F.-C. Yeh, L.M. Foley, D.J. Bain, C. Ho, Decreased reticuloendothelial system clearance and increased blood half-life and immune cell labeling for nano- and micron-sized superparamagnetic iron-oxide particles upon pre-treatment with Intralipid, Biochim. Biophys. Acta Gen. Subj. 1830 (2013) 3447–3453.
[19] R.K. Watt, R.J. Hilton, D.M. Graff, Oxido-reduction is not the only mechanism allowing ions to traverse the ferritin protein shell, Biochim. Biophys. Acta Gen. Subj. 1800 (2010) 745–759.
[20] A.R. Montazerabadi, A. Sazgarnia, M.H. Bahreyni-Toosi, A. Ahmadi, A. Shakeri-Zadeh, A. Aledavood, Mitoxantrone as a prospective photosensitizer for photodynamic therapy of breast cancer, Photodiagn. Photodyn. Ther. 9 (2012) 46–51.
[21] L.C. Tu, C.-K. Chou, C.-Y. Chen, Y.-T. Chang, Y.-C. Shen, S.-F. Yeh, Characterization of the cytotoxic mechanism of Mana-Hox, an analog of manzamine alkaloids, Biochim. Biophys. Acta Gen. Subj. 1672 (2004) 148–156.
[22] H. Chen, X. Dong, J. Shi, J. Zhao, Z. Hua, J. Gao, M. Ruan, D. Yan, Templated synthesis of hierarchically porous manganese oxide with a crystalline nanorod framework and its high electrochemical performance, J. Mater. Chem. 17 (2007) 855–860.
[23] X. Jiang, C. Rocker, M. Hafner, S. Brandholt, R.M. Dorlich, G.U. Nienhaus, Endo- and exocytosis of zwitterionic quantum dot nanoparticles by live HeLa cells, ACS Nano 4 (2010) 6787–6797.
[24] M. Mahmoudi, S. Sant, B. Wang, S. Laurent, T. Sen, Superparamagnetic iron oxide nanoparticles (SPIONs): development, surface modification and applications in chemotherapy, Adv. Drug Deliv. Rev. 63 (2011) 24–46.
[25] M.E. Huff, W.E. Balch, J.W. Kelly, Pathological and functional amyloid formation orchestrated by the secretory pathway, Curr. Opin. Struct. Biol. 13 (2003) 674–682.
[26] A. Salvati, A.S. Pitek, M.P. Monopoli, K. Prapainop, F.B. Bombelli, D.R. Hristov, P.M. Kelly, C. Åberg, E. Mahon, K.A. Dawson, Transferrin-functionalized nanoparticles lose their targeting capabilities when a biomolecule corona adsorbs on the surface, Nat. Nanotechnol. 8 (2013) 137–143.
[27] T. Kim, E. Momin, J. Choi, K. Yuan, H. Zaidi, J. Kim, M. Park, N. Lee, M.T. McMahon, A. Quinones-Hinojosa, J.W.M. Bulte, T. Hyeon, A.A. Gilad, Mesoporous silica-coated hollow manganese oxide nanoparticles as positive T 1 contrast agents for labeling and MRI tracking of adipose-derived mesenchymal stem cells, J. Am. Chem. Soc. 133 (2011) 2955–2961.